

Coherence effects in nonlinear Thomson scattering by electrons born from the same atomNuno Barros e Sá ^{*}*FCT, Universidade dos Açores, 9500-321 Ponta Delgada, Portugal*

Yance Sun and Justin Peatross

Department of Physics and Astronomy, Brigham Young University, Provo, Utah 84602, USA

(Received 29 February 2024; revised 30 August 2024; accepted 9 September 2024; published 15 October 2024)

We investigate theoretically nonlinear Thomson scattering by multiple electrons ionized from individual atoms during a short high-intensity laser pulse. The emitted light is influenced by the distance that the electrons move apart from each other during the passage of the pulse, owing to coherence effects. We examine trajectories of electrons born from the same atom via successive ionizations as the laser pulse ramps up. While the overall trajectory of an individual electron is influenced by the ponderomotive force, we find that the separation between electrons arises mostly from stronger and differing initial drift velocities associated with the moment of ionization in the laser field. In the case of helium, we find that the separation between its two ionized electrons becomes appreciable (compared to emitted wavelengths) primarily along the dimension of laser linear polarization. This distorts the angular emission patterns of nonlinear Thomson scattering in comparison with emission from individual free electrons. Radiation scattered perpendicular to the laser polarization tends to add constructively, while radiation scattered along the direction of linear laser polarization tends to add incoherently. This effect becomes more pronounced for atoms with higher numbers of ionized electrons. The effect influences primarily the lower harmonic orders.

DOI: [10.1103/PhysRevA.110.043508](https://doi.org/10.1103/PhysRevA.110.043508)**I. INTRODUCTION**

Free electrons in a sufficiently intense laser field can emit harmonic radiation through nonlinear Thomson scattering. A classical understanding of this process began in 1951 when Landau and Lifshitz showed that electrons should execute figure-8 motion in a linearly polarized plane wave if the intensity is sufficient to drive relativistic motion [1]. Vachaspati pointed out in 1962 that electrons undergoing such motion will radiate both odd and even harmonics [2]. In 1970, Sarachik and Shappert published a landmark theoretical treatment of classical nonlinear Thomson scattering [3]. The theoretical analyses of light scattering from laser-driven free electrons at relativistic intensities have been revisited by many researchers since [4–18].

Experimental measurements have often used energetic electron beams that collide with laser pulses [19–26]. This results in Lorentz-boosted scattering in the form of highly directional beams of x rays. Relatively few measurements have been made of nonlinear Thomson scattering from electrons that drift only modestly relative to the laboratory frame [27–30]. The low cross section of electron-photon interactions requires thousands of free electrons in a laser focus to make a measurement, but the density should be low enough to avoid interactions between, for example, electrons and parent ions if used to donate the free electrons.

We recently reported on the angular distribution and polarization of fundamental, second-harmonic, and third-harmonic

light scattered from electrons ionized from low-density helium [31,32]. In the analysis of that data, we summed incoherently the emission from ionized electrons without regard for the common initial position of electron pairs born from individual atoms during the laser pulse. In this paper, we consider how multiple electrons ionized from the same atom can produce coherence effects in emitted nonlinear Thomson scattering.

The possibility that the ionization process imprints coherence effects on the photoemission from multiple electrons freed from the same atom may provide further insights into strong-field ionization. Indeed, whether the quantum probability current of ionizing electrons emerges from atoms over several laser cycles or more abruptly during a rapidly increasing laser field is a topic of interest [33–39]. Moreover, coherence effects in the photoemission from multiple-electron quantum wave packets driven by an ultraintense laser field have been the topic of recent theoretical investigation [40].

We explore the extent to which the radiation scattered from free electrons originating from the *same* atom will be coherent, and whether the coherence, when present, will exhibit angular dependence. In essence, the answer to this problem amounts to estimating the relative positions of electrons when they emit radiation. If their separation remains small compared to the scattered wavelength, then obviously their radiation will be coherent, but as we shall see, this is not always the case.

II. COHERENCE

We summarize briefly coherence effects in the radiation emitted from two electrons. Let \vec{k}_i and \vec{k}_s be the wave vectors

^{*}Contact author: nuno.bf.sa@uac.pt; peat@byu.edu; Also at Instituto de Astrofísica e Ciências do Espaço, 1349-018 Lisboa, Portugal.

of the incident and scattered radiation respectively, and \vec{d} the difference in position between two electrons when they emit radiation. The directionally dependent phase difference of their emissions is

$$\Delta\phi = (\vec{k}_s - N\vec{k}_i) \cdot \vec{d} = \frac{2\pi N}{\lambda} (\hat{e}_s - \hat{e}_i) \cdot \vec{d}, \quad (1)$$

where N is the harmonic order of the emission and λ is the wavelength of the incident radiation. In our earlier experiments [31,32], N is slightly smaller than the harmonic order due to a redshift caused by a forward drift of electrons during the laser interaction. In Eq. (1), \hat{e}_s and \hat{e}_i refer to the direction of the scattered light and that of laser propagation, respectively. The redshift is more pronounced for emission in directions that are farther from the direction of laser propagation.

Constructive interference occurs for a phase difference up to $\pi/2$, or, equivalently, if

$$\frac{\lambda}{4(\hat{e}_s - \hat{e}_i) \cdot \vec{d}} > N \quad (2)$$

where we have used the replacement $k_s = 2\pi N/\lambda$. For scattering in the forward direction this condition is automatically satisfied, since $\hat{e}_s - \hat{e}_i$ is tiny. In this particular direction, a much stronger beam occurs due to constructive interference between all electrons in the interaction region.

Notice, however, that emission is influenced by electron separation along the direction of observation \vec{d} as well as by the time delay between the interactions of the laser field with each electron. The former effect is governed by $\vec{k}_s \cdot \vec{d}$ and the latter by $\vec{k}_i \cdot \vec{d}$ in Eq. (1). That is, coherent emission occurs when $(\vec{k}_s - N\vec{k}_i) \cdot \vec{d}$ is small, either because \hat{e}_s and \hat{e}_i are aligned, because the electrons are close together such that \vec{d} is small, or because the dot product is small on account of orthogonality.

In this paper, we will make the approximation that electrons immediately become free upon ionization, since the electric field of the laser dominates as electrons move only a tiny fraction of a laser wavelength away from their parent ions. In addition, during a laser pulse lasting a few tens of femtoseconds, atoms and ions move imperceptibly compared to a laser wavelength, so they may be thought of as remaining essentially at the same position during the multiple ionizations. Finally, after becoming free, electrons pick up kinetic energy from the laser field that far surpasses their ionization potentials. Therefore, it is reasonable to neglect any intrinsic velocity that an electron may possess as it first detaches from its parent ion. Please note the distinction between the initial velocity of an electron upon ionization that we mention here and the concept of “drift velocity” to be used later (Sec. IV), which refers to the mean velocity (averaged over a cycle) that a free electron can acquire in the gradient of a laser pulse.

III. IONIZATION

The probability that an electron has become ionized from its parent atom at any moment during a laser pulse may be written

$$P(t) = 1 - e^{-\int_{-\infty}^t W(s) ds} \quad (3)$$

where $W(t)$ is the ionization rate, which inherits time dependence through the local laser field. The probability that an electron becomes ionized within time interval Δt is then

$$\Delta P \cong W(t) e^{-\int_{-\infty}^t W(s) ds} \Delta t. \quad (4)$$

In this paper, once an electron becomes ionized, we will treat it classically. This is justified both theoretically [41–43] and experimentally [44] by the fact that an electron quantum wave packet driven by an electromagnetic plane wave emits with the strength of a classical point emitter, independent of its spatial extent (i.e., the size of its spreading wave packet).

The simplest model for ionization is an instantaneous one, where electrons are completely bound until a threshold electric field is achieved, whereupon the electron is suddenly released. In this case, the ionization probability density might be written as

$$\frac{d}{dt} P(t) = \delta(t - t_I) \quad (5)$$

where t_I is the earliest moment when a critical field is achieved. An estimate for this field may be obtained classically from the suppression of a Coulombic barrier, i.e., barrier suppression ionization (BSI) [33]:

$$E_{\text{cr}} = \frac{\pi \epsilon_0 \Phi^2}{Z e^3}. \quad (6)$$

Here Z is the charge state of the ion or atom, and Φ is the binding energy of the electron that is ionized.

We will also employ the widely used Ammosov-Delone-Krainov (ADK) model of ionization [45,46]. For this model, the ionization rate is

$$W_{\text{ADK}} = \frac{\Phi}{\hbar} C_{kl}^2 (2l+1) \left(\frac{2}{F}\right)^{2n^* - |m| - 1} \times \frac{(l+|m|)!}{2^{|m|} |m|! (l-|m|)!} \exp\left(-\frac{2}{3F}\right). \quad (7)$$

Here n , l , and m are the orbital quantum numbers, and $n^* = Z\sqrt{\Phi_a/(2\Phi)}$ is the effective principal quantum number of the atom or ion. In the above formula, we have

$$F = \frac{E}{E_a} \left(\frac{\Phi_a}{2\Phi}\right)^{3/2}, \quad (8)$$

$$C_{kl}^2 = \frac{2^{2n^*}}{n^* \Gamma(n^* + l^* + 1) \Gamma(n^* - l^*)} \quad (9)$$

where $l^* = n_0^* - 1$ is an effective orbital quantum number, calculated from the effective principal quantum number of lowest state with the given quantum number l [47]. Finally, the above formulas include the characteristic atomic energy Φ_a and electric field E_a . These are defined by

$$\Phi_a = \frac{m_e e^4}{(4\pi \epsilon_0)^2 \hbar^2}, \quad (10)$$

$$E_a = \frac{m_e^2 e^5}{(4\pi \epsilon_0)^3 \hbar^4}. \quad (11)$$

Figure 1 shows the probability of ionization per time calculated for helium using the ADK model together with the electric-field intensity expressed in terms of the dimensionless

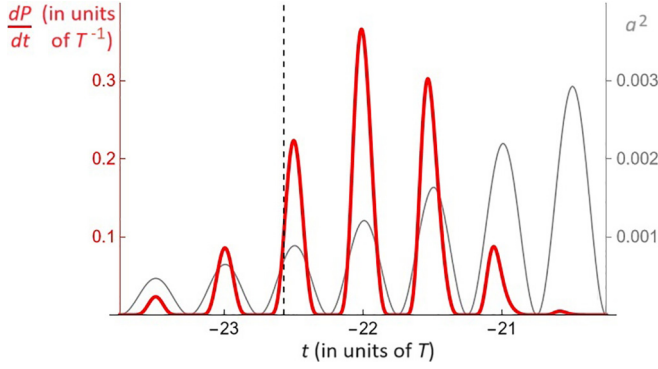


FIG. 1. Probability per time, $\Delta P/\Delta t$ (thick red line), given by Eq. (4), for the first ionization of helium using ADK. The thin gray line represents the square of the electric field (i.e., instantaneous intensity) expressed in terms of the dimensionless quantity a^2 . The dashed vertical line marks the instant when ionization would occur in the instantaneous model, i.e., when barrier suppression is achieved. Time is in units of laser periods T with $t = 0$ corresponding to the local peak of the laser pulse.

parameter

$$a = \frac{eE}{km_e c^2}. \quad (12)$$

This probability density was calculated using a laser pulse with the characteristics described in the next section, assuming the helium atom is located at the center of the laser focus. Ionization occurs mostly within the first two half periods after E_{cr} is reached. Also note that most ionization occurs around the peaks of the laser oscillations.

As will become evident later in this paper, the calculated nonlinear Thomson scattering is not overly sensitive to the details of the ionization model used to produce the free electrons that subsequently scatter the light. The essential ingredient is that ionization happens over several laser oscillations during an expected intensity range, which typically occurs several orders of magnitude below the intensity required for nonlinear Thomson scattering. Electrons ionized by the less realistic instantaneous model exhibit modest differences in their coherence relative to electrons ionized more gradually. Of course, for simulations using classical point electrons, gradual ionization is incorporated through ensemble averaging with different moments of ionization as dictated by the probability curve.

IV. ELECTRON TRAJECTORIES

The equation of motion for a free classical pointlike electron subject to a laser field is

$$\frac{d}{dt}(\gamma\vec{v}) = \frac{-e}{m_e}(\vec{E} + \vec{v} \times \vec{B}), \quad (13)$$

where \vec{E} and \vec{B} are the laser electric and magnetic fields, and \vec{v} is the electron velocity. The equation is solved for electron position $\vec{r}(t)$ subject to the condition that, at the instant of ionization t_I , the velocity of each electron is zero, and electrons born from the same atom share the same initial position. Solving these equations, we can find the separation \vec{d} as a function of time between two sibling electrons released from

a parent atom during the rising edge of a pulse. This will allow us to investigate the coherence behavior indicated in Eq. (2).

We consider only linearly polarized incident radiation. For our calculations, we employ the model for an x -polarized laser pulse moving along the z direction used in Ref. [31], namely [48,49]

$$\vec{E} = \text{Re} \left\{ E_0 e^{-\left(\frac{\omega}{c}\right)^2 \left(\hat{x} + \frac{xy}{2\mathbb{Z}^2} \hat{y} - i \frac{x}{\mathbb{Z}} \hat{z} \right)} \times \frac{z_0}{\mathbb{Z}} e^{-\frac{kz_0}{2|\mathbb{Z}|^2} (x^2 + y^2)} e^{i(\varphi + \varphi_0)} \right\}, \quad (14)$$

where $\mathbb{Z} = z_0 + iz$ and $\varphi = kz[1 + (x^2 + y^2)/(2|\mathbb{Z}|^2)] - \omega t$ and φ_0 is an initial phase. The Rayleigh range z_0 relates to the radius of the focus w_0 through $z_0 = kw_0^2/2$; τ is the pulse duration; ω and k have the usual meanings of angular frequency and wave number. The associated magnetic field is $\vec{B} = (E_y/c)\hat{x} + (E_x/c)\hat{y} + (E_z/c)(y/x)\hat{z}$.

In our analysis, we will use the following prototypical experimental values [31]:

$$\lambda = 800 \text{ nm}, \quad (15)$$

$$a_0 = \frac{eE_0}{km_e c^2} = 1 \quad (I = 2.1 \times 10^{18} \text{ W/cm}^2), \quad (16)$$

$$w_0 = 4\lambda = 3.2 \text{ } \mu\text{m}, \quad (17)$$

$$\tau = 12T = 12 \frac{\lambda}{c} = 32 \text{ fs}. \quad (18)$$

Free-electron trajectories can be described as the superposition of two movements (see Fig. 2): an oscillating component, performing a figure-8 movement in response to the driving pulse [3,27,31,50], and an overall drift movement both along the direction of laser propagation and outward from the laser axis due to ponderomotive forces. The latter can influence the separation between electrons born from the same atom during the passage of the pulse. However, ponderomotive forces tend to be similar for sibling electrons, and their separation is often governed mostly by different initial drift velocities associated with the phases and field strengths upon ionization, at least until the peak of the laser pulse when electrons undergo nonlinear Thomson scattering. Note that the onset of nonlinear Thomson scattering is characterized by $a \approx 1$.

Figure 2 shows the x , y , and z components of a single electron trajectory starting from an arbitrary position in the focus. One can notice the effect of an initial drift velocity along the direction of laser polarization (x dimension), required for an electron to be at rest upon release at a particular phase of the laser field, in accordance with assumptions at the end of Sec. II. This initial drift is the same that gives rise to, for example, the plateau cutoff of high harmonics [51]. After a time, the electron also acquires velocities in the y and z directions, owing to Lorentz-force drift and lateral ponderomotive forces. Along the z direction, both the oscillatory motion and the initial drift velocity are small on the scale shown, while along the y direction oscillations and initial drift velocity are both essentially zero. On the other hand, the direction of laser polarization (x) exhibits strong oscillations and higher initial drift velocity.

Figure 3 compares trajectories for a pair of electrons ionized from a helium atom located at the same point used in

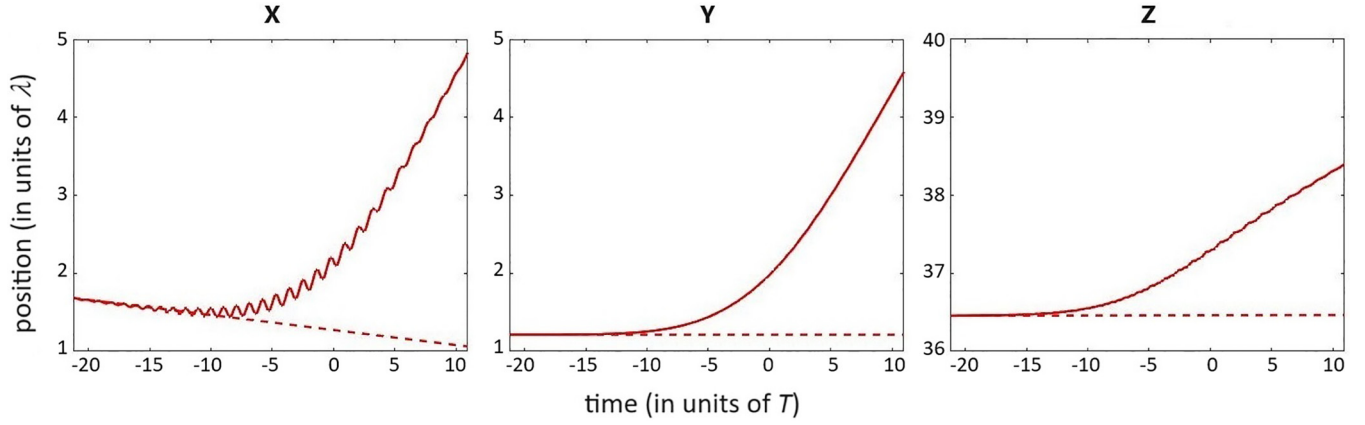


FIG. 2. Trajectory of an electron along the x , y , and z axes, with an arbitrary initial position, calculated numerically using Eqs. (13) and (14). The dotted lines represent the initial drift velocity, calculated using Eqs. (19) and (20). The time axis is adjusted so that $t = 0$ corresponds to the pulse peak at the parent atom.

Fig. 2. Relevant to this paper is how soon the electrons significantly separate from each other as they interact with the laser field. The larger separation acquired along the x axis (direction of polarization) is primarily due to the different initial drift velocities of the two electrons when they are born. Notice that the separation between the electrons along the directions perpendicular to the polarization remains small compared to the wavelength (1 on this scale) until after the peak of the pulse (at $t = 0$).

In Table I, we show the results of a numerical simulation, using Eqs. (13) and (14), for helium. The table shows the average separation between its two electrons at the local peak of the laser pulse. The computation was made using an ensemble of 1000 electrons, randomly distributed throughout the interaction region, that is within a cylinder centered on the focus with radius w_0 and length $2z_0$. This is done for both the ADK and instantaneous ionization models. The table also shows the average time Δt between ionization and the local pulse peak, as well as components of the average initial drift velocity for each of the two electrons. From Table I, one can appreciate that separation between the electrons along the y and z dimensions, d_y and d_z , is an order of magnitude smaller than the separation along the x dimension, d_x .

V. ESTIMATE OF TRAJECTORY SEPARATION

The initial drift velocity is an important factor affecting the spatial separation between electrons. Depending on the exact moment that the electron breaks free from its atom, it inherits an initial velocity. This initial velocity ensures that the electron starts out at rest while oscillating with the particular phase of the field. The initial drift velocity is given by [14,52]

$$v_{0x} = -2c \frac{(a_I/2) \sin \theta_I}{1 + (a_I/2)^2 (1 + 2 \sin^2 \theta_I)}, \quad (19)$$

$$v_{0y} = 0, \quad (20)$$

$$v_{0z} = c \frac{(a_I/2)^2 (1 + 2 \sin^2 \theta_I)}{1 + (a_I/2)^2 (1 + 2 \sin^2 \theta_I)}, \quad (21)$$

where a_I and θ_I are the strength, measured by Eq. (12), and phase of the field at the moment of ionization. Whatever model is used for ionization, we expect it to occur within a few half periods of the instant when the critical field is reached, used in the instantaneous model of ionization. We therefore estimate the field strength with $a_I \approx a_{cr}$. Further, the ionization states that we consider have $a_I \ll 1$. We therefore neglect the corrections in the denominator of Eqs. (19)–(21).

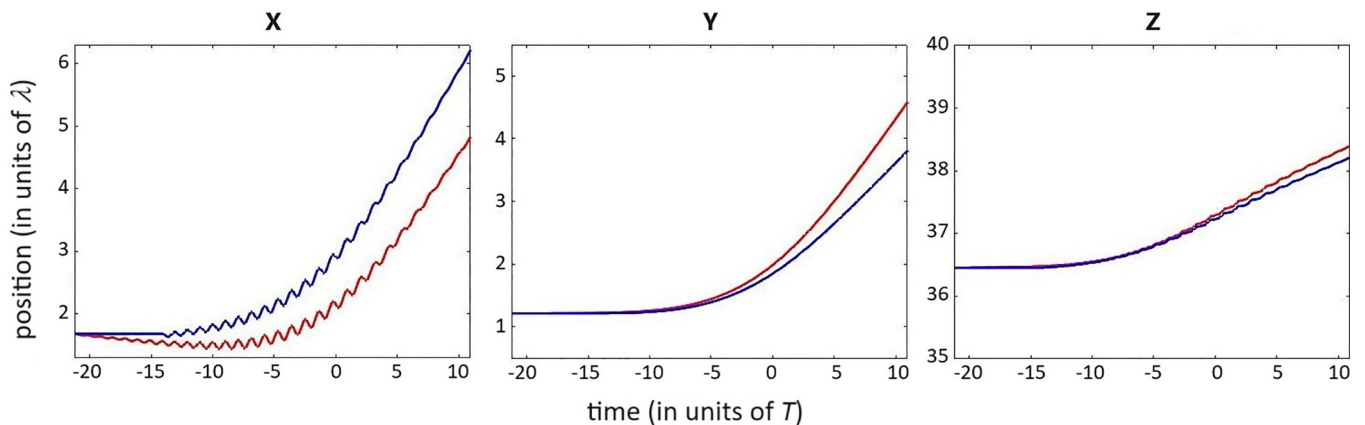


FIG. 3. Trajectories along the separate axes of two electrons coming out from the same helium atom: first, red (light line in grayscale); second, blue (dark line).

TABLE I. Time of ionization (prior to local pulse peak, in units of T) and initial drift velocities (in units of c) for the two electrons of helium, and their separation (in units of λ) at the instant of maximum field strength. The table shows averages from 1000 electrons randomly distributed inside a cylinder centered on the laser focus. INST stands for ionization occurring exactly at the instant when $a = a_{\text{cr}}$; ADK is given by the rate (7). The theoretical estimate TE is computed following the results of Sec. V.

	ADK	INST	TE
Δt_1	20.0	21.0	20.6
Δt_2	17.0	17.6	17.2
v_{1x}	0.0113	0.0096	0.0131
v_{1z}	0.0004	0.0002	0.0003
v_{2x}	0.0251	0.0225	0.0320
v_{2z}	0.0019	0.0014	0.0015
d_x	0.412	0.342	0.581
d_y	0.052	0.043	
d_z	0.046	0.054	

Moreover, taking $\langle |\sin \theta_I| \rangle \approx 1/2$, as we are mostly interested in obtaining an order of magnitude and not an exact value, one ends up with

$$\langle |v_{0x}| \rangle = \frac{1}{2} c a_{\text{cr}}, \quad (22)$$

$$\langle |v_{0z}| \rangle = \frac{3}{8} c a_{\text{cr}}^2 \quad (23)$$

where a_{cr} is calculated using the field strength E_{cr} .

For not too large values of the coordinates x , y , and z of the parent atom, one can approximate the envelope of the pulse Eq. (14) by

$$E \sim E_0 \exp \left[-\frac{(z/c - t)^2}{\tau^2} \right] \frac{z_0}{\sqrt{z^2 + z_0^2}} \exp \left(-\frac{x^2 + y^2}{w_0^2} \right). \quad (24)$$

Peak field intensity at the parent atom occurs at $t = z/c$, and thus

$$E \sim E_0 \exp \left(-\frac{\Delta t^2}{\tau^2} \right) \frac{z_0}{\sqrt{z^2 + z_0^2}} \exp \left(-\frac{x^2 + y^2}{w_0^2} \right), \quad (25)$$

with Δt the time difference between the instant in consideration and the instant of peak intensity. For the purpose of averaging, we take

$$\begin{aligned} & \left\langle \frac{z_0}{\sqrt{z^2 + z_0^2}} \exp \left(-\frac{x^2 + y^2}{z_0^2} \right) \right\rangle \\ &= \frac{\int_{-z_0}^{z_0} dz z_0 (z^2 + z_0^2)^{-1} \int_0^{w_0} d\rho 2\pi \rho e^{-\rho^2/w_0^2}}{\int_{-z_0}^{z_0} dz \int_0^{w_0} d\rho 2\pi \rho} \approx 0.5 \end{aligned} \quad (26)$$

and get, from Eq. (25),

$$E \sim \frac{E_0}{2} \exp \left(-\frac{\Delta t^2}{\tau^2} \right). \quad (27)$$

The time elapsed between the instant of ionization and the instant of highest field intensity at the parent atom is then

obtained by setting $E = E_{\text{cr}}$ in Eq. (27) to get

$$\Delta t = \tau \sqrt{\ln \left(\frac{a_0}{2a_{\text{cr}}} \right)}. \quad (28)$$

Again, this result is a rough estimate without regard for a specific ionization model.

For the parameters (15)–(18) we have $a_{\text{cr}} = 0.026$ and 0.064 for the two electrons of helium. v_{0z} is therefore small and can be ignored. Along the x direction the position of each electron at the moment of highest field intensity is $x + v_{0x} \Delta t$ and the distance between the two electrons is

$$\begin{aligned} d_x &= \left| (x + v_{0x}^{\text{second}} \Delta t^{\text{second}}) - (x + v_{0x}^{\text{first}} \Delta t^{\text{first}}) \right| \\ &= \left| v_{0x}^{\text{second}} \Delta t^{\text{second}} - v_{0x}^{\text{first}} \Delta t^{\text{first}} \right| \end{aligned} \quad (29)$$

where the superscripts “first” and “second” stand for the first and second electrons.

Moreover, since a_{cr} grows with Φ^2/Z , it is larger for the second electron than for the first, therefore typically $|v_{0x}^{\text{second}}| > |v_{0x}^{\text{first}}|$. This together with $\Delta t^{\text{second}} \approx \Delta t^{\text{first}}$ means that the separation between the two electrons is determined primarily by the velocity of the second one:

$$d_x \approx \langle |v_{0x}| \rangle \Delta t \text{ (second electron)}. \quad (30)$$

By combining Eqs. (28) and (30), we arrive at

$$d_x = \frac{c a_{\text{cr}}}{2} \tau \sqrt{\ln \left(\frac{a_0}{2a_{\text{cr}}} \right)}, \quad (31)$$

where a_{cr} is to be computed for the latest electron.

As seen in Table I, the agreement of this analytical estimate with the numerical results is perhaps better than it should be, given that it is intended merely to obtain the correct order of magnitude. It underscores that the result is not sensitive to the exact ionization model used. The ADK model, which permits ionization over several half laser cycles after a_{cr} is reached, produces slightly smaller values of Δt and slightly larger values for separations and velocities than the instantaneous model. The fact that our theoretical estimate does not produce smaller values for the separation and velocity along x is due in part to our arbitrary choice of the value $1/2$ for $\langle \sin \theta_I \rangle$; still, the order of magnitude is likely correct.

VI. NONLINEAR THOMSON SCATTERING

We computed the classical radiation emitted by the accelerated electrons following the same approach as described in Ref. [31]. The far-field radiation pattern is dictated by [53]

$$\vec{E}_{\text{rad}} = \frac{q}{4\pi\epsilon_0 c^2 R} \frac{\hat{R} \times [(\hat{R} - \vec{u}/c) \times \vec{a}]}{(1 - \hat{R} \cdot \vec{u}/c)^3}, \quad (32)$$

where R is the distance from the interaction region to a detector and $\hat{R} = \hat{x} \sin \theta \cos \phi + \hat{y} \sin \theta \sin \phi + \hat{z} \cos \theta$ is a unit vector specifying the direction to that detector. The right-hand side of (32) is evaluated at (retarded) time t , whereas the left-hand side is a function of detector time $t' = t - \hat{R} \cdot \frac{\vec{r}}{c}$, ignoring an overall constant time delay R/c .

We consider separately scattered photons with *longitudinal* and *azimuthal* polarization, aligned along $\hat{\theta} = \hat{x} \cos \theta \cos \phi + \hat{y} \cos \theta \sin \phi - \hat{z} \sin \theta$ or along $\hat{\phi} = -\hat{x} \sin \phi + \hat{y} \cos \phi$. These

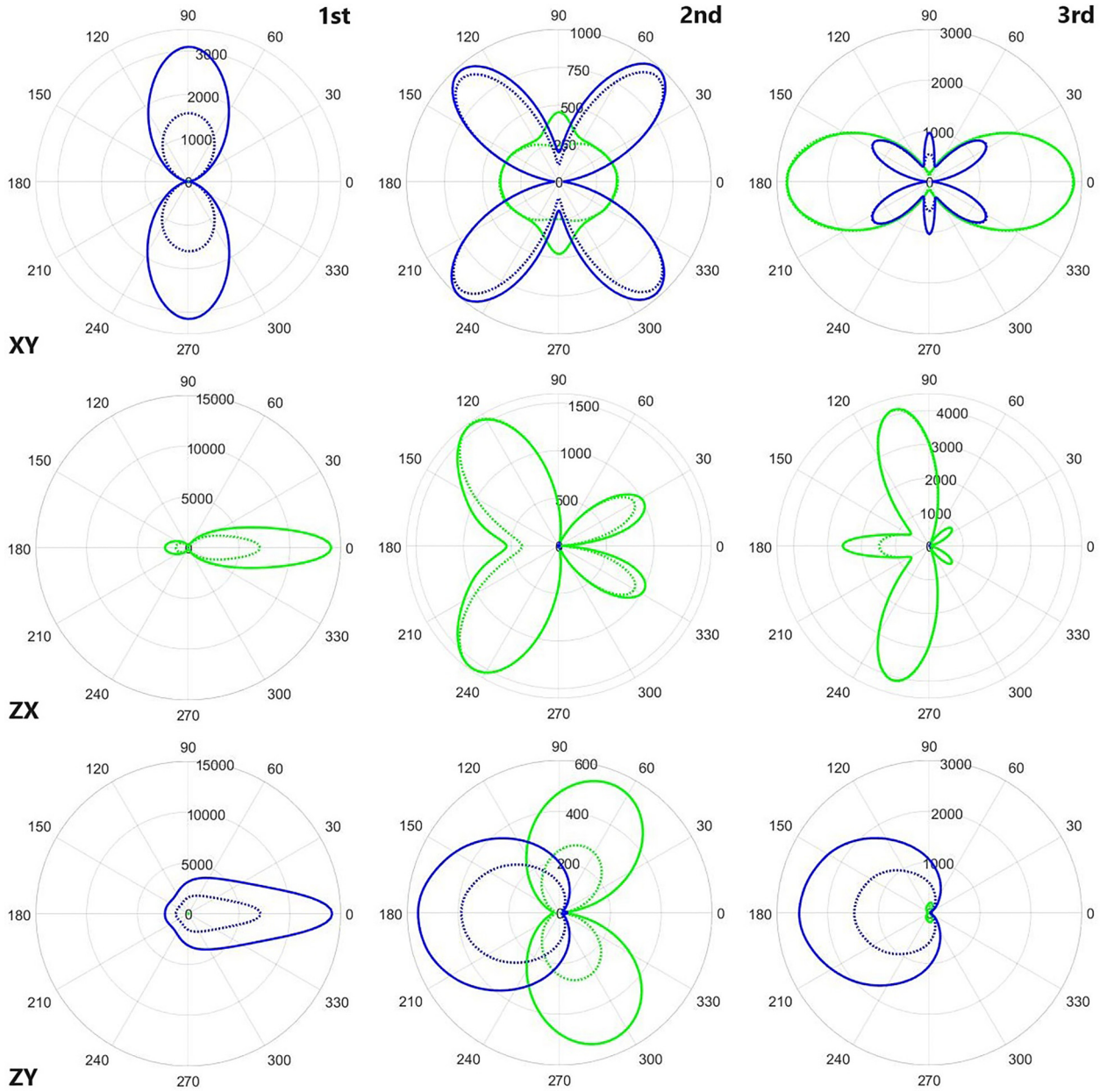


FIG. 4. Far-field angular distribution of photon counts along three planes for first, second, and third harmonics. Blue (dark line in grayscale) stands for the radiation with azimuthal polarization (parallel to the XY plane) and green (light line) stands for longitudinal polarization (orthogonal to azimuthal). The full lines indicate the photon counts computed while allowing for interference between pairs of electrons. The dotted lines indicate photon counts while ignoring interference (i.e., summing intensities). In the top row, the horizontal axis is the x axis. In the other rows, the horizontal axis is the z axis.

are the usual unit vectors in spherical coordinates, perpendicular to \hat{R} . The total energy per steradian (angular fluence) is $\Phi_\theta + \Phi_\phi$ where $\Phi_\theta = \epsilon_0 c R^2 \int_{-\infty}^{\infty} |\hat{\theta} \cdot \vec{E}_{\text{rad}}|^2 dt'$ and $\Phi_\phi = \epsilon_0 c R^2 \int_{-\infty}^{\infty} |\hat{\phi} \cdot \vec{E}_{\text{rad}}|^2 dt'$. A polarizer in front of the detector, aligned along either $\hat{\theta}$ or $\hat{\phi}$, would transmit either Φ_θ or Φ_ϕ .

The Fourier transform of \vec{E}_{rad} may be taken and a desired spectral window applied to restrict to a specific harmonic. To explore theoretically emission over the entire emission sphere, we adjust the center of numerical bandpass filters to account for different redshifts of the harmonic emission, depending on

the polar angle θ measured relative to the direction of laser propagation. We adjust the center wavelength of the bandpass filter for the N th harmonic to the redshifted peak intensity [54,55]:

$$\lambda_N(\theta) = \left(1 + \frac{1}{2} a_0^2 \sin^2 \frac{\theta}{2}\right) \frac{\lambda}{N}. \quad (33)$$

In our calculations, we make the replacement $a_0 \mapsto a_0/2$ in this formula to account for averaging in the spirit of Eq. (26). We use filters with bandwidth $\Delta\lambda_N = \lambda_N/20$.

We consider radiation emanating from a cylinder with radius w_0 and length $2z_0$, centered on the laser focus. We

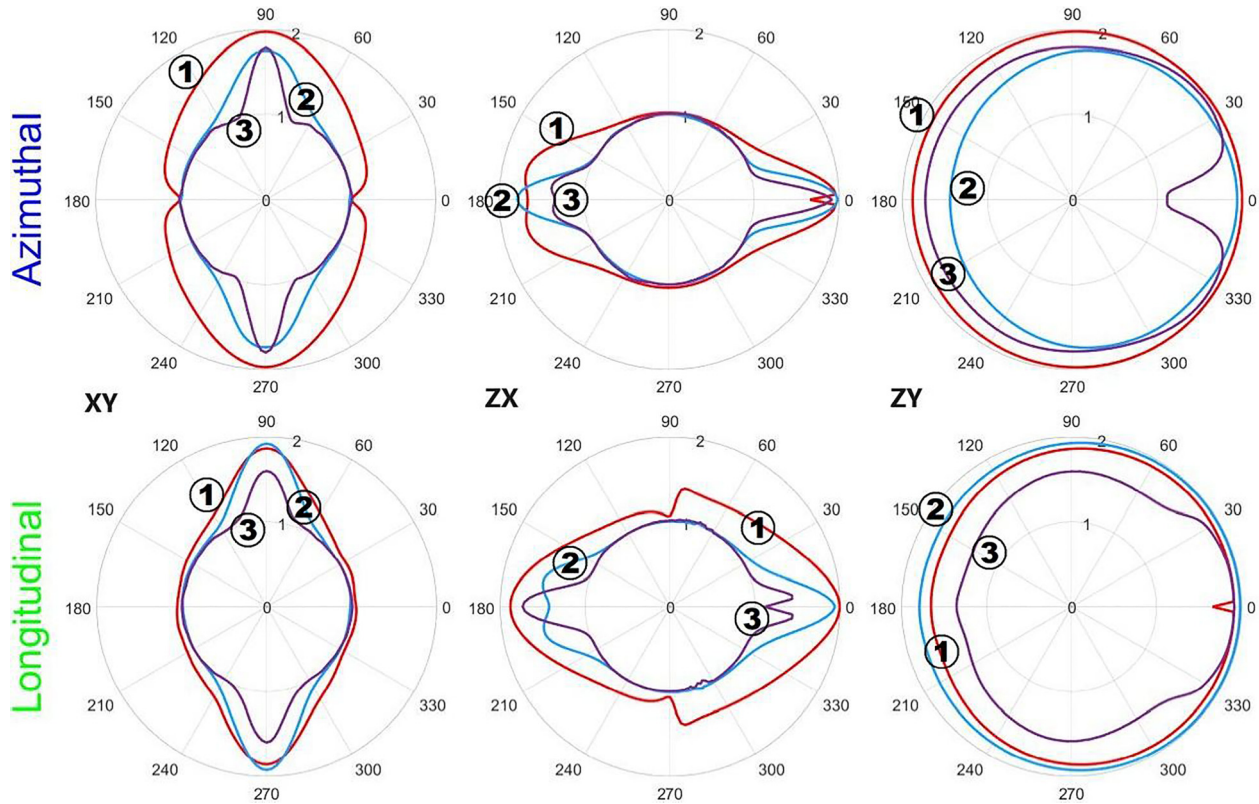


FIG. 5. Ratio of curves seen in Fig. 4, namely, a comparison between simulations with and without the possibility of interference between emission from electron pairs. Red lines represent the fundamental, blue lines represent the second harmonic, and purple lines represent the third harmonic—labeled 1, 2, and 3, respectively.

assume the same gas pressure photon-collection and detection efficiency as in Ref. [31]. The number of photons emitted within a solid angle of 0.15 sr after 1000 laser pulses is plotted in Fig. 4 along the three planes XY , ZY , and ZX , and compared with the number of photons that would have been obtained if no interference was present between the pairs of electrons from each helium atom. The latter is essentially the same as for free electrons. To compute the interference, we sum the amplitudes of the fields radiated by the two electrons of each atom and then square it. The no-interference case is obtained by first squaring the fields before adding them. Then we average (incoherently) over 10 000 atoms randomly distributed in the interaction region. We show the results for each of the first three harmonics ($N = 1, 2, 3$).

In Fig. 5 we plot the ratio of photon counts with and without interference for the fundamental, second, and third harmonics. The variation in the curves is a kind of measure of the amount of interference. A value of 1 indicates incoherence, and a value of 2 indicates perfect coherence. As can be seen, whether the emission is coherent or incoherent highly depends on the direction of emission. This, of course, depends on the dimension along which the two electrons ionized from helium become separated.

VII. HIGHER-Z ATOMS

One may expect that, employing atoms with higher numbers of electrons, the effect of coherence between ionized

electrons will be strongly enhanced. This is implied by the theoretical estimate (31). In this section, we compare simulations of nonlinear Thomson scattering from free electrons ionized from helium vs argon in the equatorial plane. We revert to filters used in Ref. [31].

In Fig. 6, we compare for helium the angular plots of scattered photons obtained using the instantaneous model of ionization given by Eq. (5) and the ADK model given by (7). We notice that the few extra half periods that it takes for atoms to ionize under the ADK model allow electrons to break free at intensities slightly greater than the critical intensity, leading to higher initial drift velocities and separations between ejected electrons. This somewhat diminishes coherence. Still, the results are not strongly influenced by the ionization model; the effects on coherence are visible but small.

The first two rows in Fig. 7 show plots made for electrons ionized from argon, under the same conditions as done for helium in Fig. 6. Up to ten electrons can be ionized from argon under the conditions simulated (though the last two with small probabilities). Our expectation that coherence effects should be enhanced appears to be validated. Moreover, the results remain not overly sensitive to the ionization model used.

It is suspected that the ADK model loses accuracy at intensities above the critical (BSI) intensity, but currently there is not one widely accepted model for this regime. We have tried three ionization models designed for the BSI regime (Fig. 8). We repeated our simulations using an adjustment to

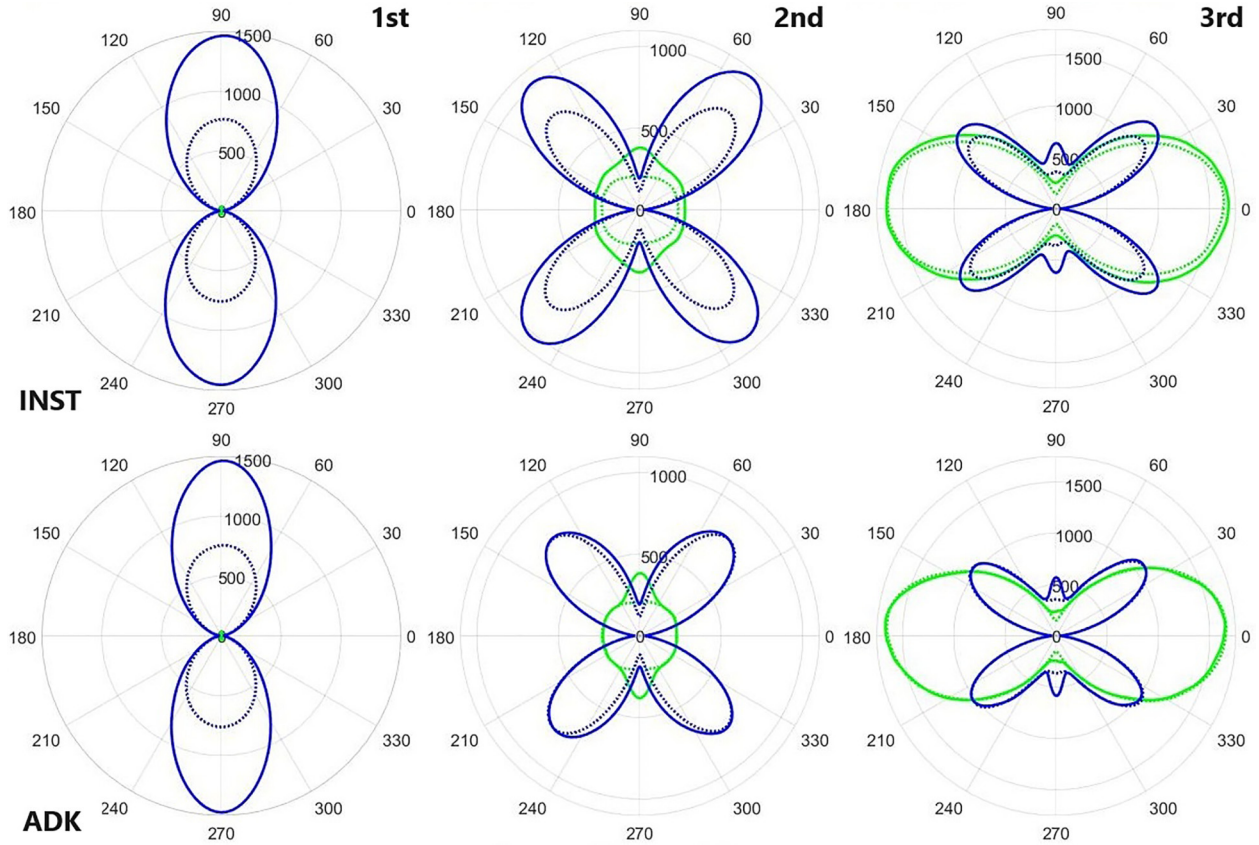


FIG. 6. Angular distributions of the fundamental, second-, and third-harmonic photon counts scattered by electrons ionized from helium, comparing the instantaneous (upper row) and ADK ionization models (lower row). The plots show scattering in the XY plane (x being the horizontal direction) using a simulation of 10 000 atoms randomly distributed throughout the same interaction region as used for Fig. 4. Blue lines indicate azimuthal polarization and green lines indicate longitudinal polarization (respectively dark and light lines in grayscale). The ADK row is a repeat of the upper row of Fig. 4, except that in this figure we use spectrally fixed bandpass filters, the same as used in Ref. [31] (centered on slightly redshifted wavelengths).

the ADK ionization rate proposed in [36], which produces results very similar to the ones obtained using the ADK model. The proposed adjustment to ADK in [38], on the other hand, noticeably suppresses coherence effects owing to releasing electrons at higher intensities. Finally, the model in [37] lies in between these two cases. We added the plots for this latter model in Fig. 7 for comparison. In general, the longer the electrons remain bound to their atoms, above the critical (BSI) intensity, the more rapidly electrons born of the same atom move apart from each other.

VIII. DISCUSSION

We have analyzed nonlinear Thomson scattering from multiple electrons ionized from the same atom. We found that coherence between these electrons should be taken into account, and that it can influence the angular distribution of the radiation, owing to the details of the trajectories that electrons follow after ionization. Coherence effects are more pronounced at the longer wavelengths such as the scattered fundamental or second harmonic. The results depend only mildly on the ionization model chosen.

Atomic species can have a significant influence on the angular distribution of scattered photons. The fundamental

and harmonics show a strong enhancement of emission from argon over helium along directions perpendicular to the laser polarization, as would be expected owing to the larger number of electrons available for ionization in argon. Concerning the possibility of verifying experimentally these phenomena, the difference in shape of the angular distribution of the higher harmonics between the cases of helium and argon should certainly be possible to observe.

As for the fundamental, the emission in the direction perpendicular to laser polarization should be approximately $4^2 = 16$ times higher for argon compared to helium at the same gas density. On the other hand, if the emission is incoherent, then the emission for argon would be only four times higher (since helium releases two electrons while argon releases about eight); this too should be observable. Moreover, the ratio between the scattered fundamental in the XY plane at 90° and 60° should be 1.33 if all free electrons are incoherent, whereas the ratio should be 1.8 for helium and 2.25 for argon if electrons born of the same atom are spatially correlated through the ionization process.

These observations about the fundamental show some dependence on the ionization model, both for helium and for argon, while the predictions for the second and third harmonics show a higher dependence on ionization model. These

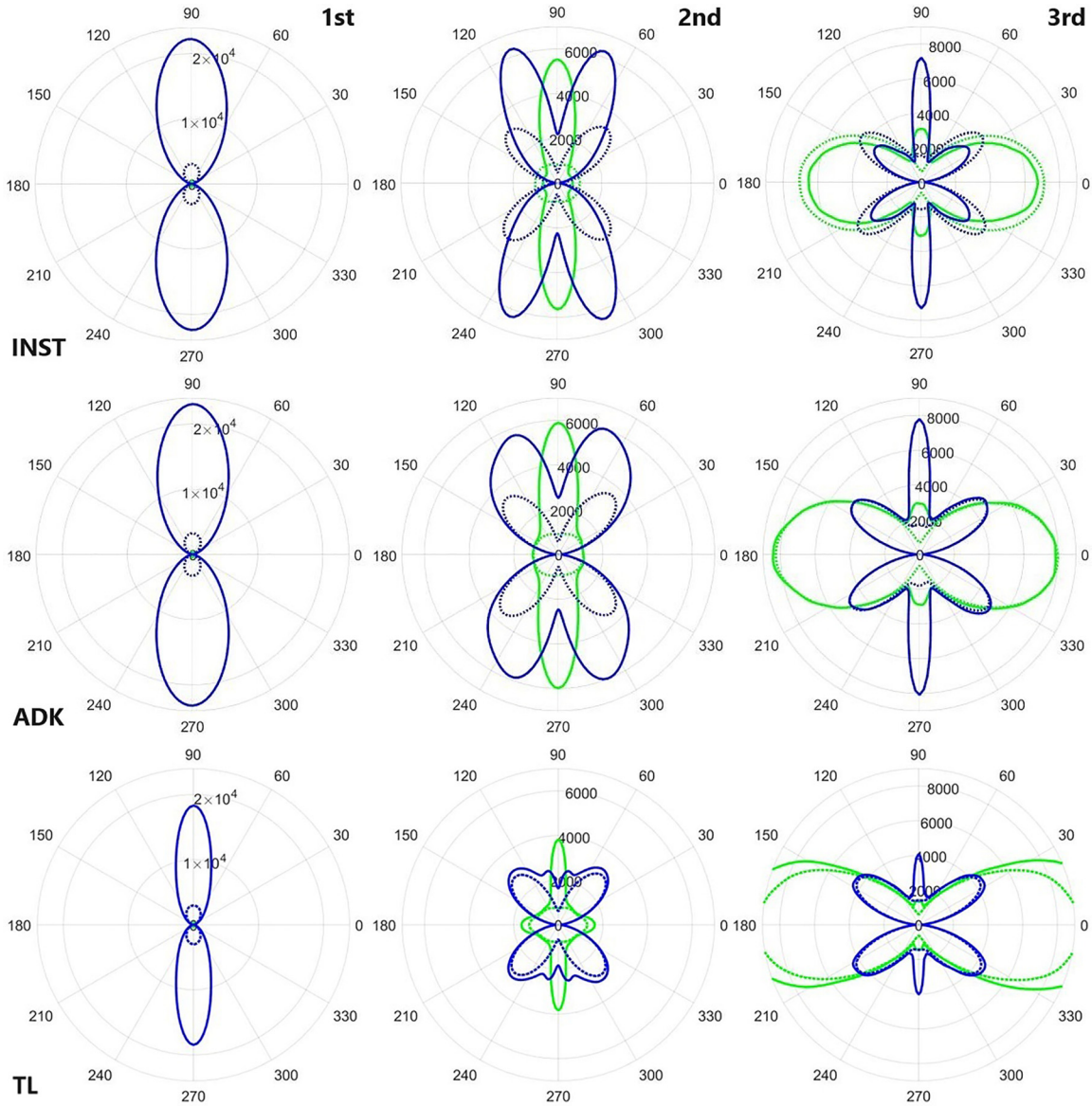


FIG. 7. Same as Fig. 6, except computed using argon. We added a third row with plots for the model by Tong and Lin [37].

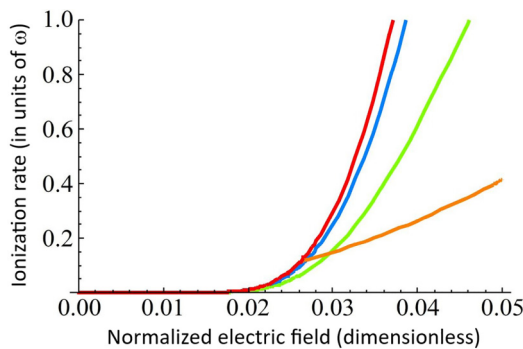


FIG. 8. Ionization rate for the first ionization of helium (in units of the angular frequency ω) as a function of electric-field intensity [measured using the dimensionless parameter a given by Eq. (12)] for four different ionization models. From left to right (that is, from the ones with higher ionization rates to the ones with lower rates): ADK (red) and the models in Refs. [36] (blue), [37] (green), and [38] (red, same as ADK, before the critical intensity, and orange after it).

variations in the angular emission pattern might be used to try to distinguish between different ionization models. In particular, observation of the distorted angular patterns predicted by us could serve to test ionization models with relatively slow ionization rates [37–39].

The angular emission could also be explored, in principle, with and without a prepulse that has sufficient intensity to ionize the gas (allowing time for electrons ionized from the same atom to decohere) but with significantly less intensity than a primary pulse that afterwards produces nonlinear Thomson scattering.

IX. CONCLUSIONS

In summary, our simulations predict measurable coherence effects in nonlinear Thomson scattering from electron bunches born of the same atoms in an intense short laser pulse. Observing these effects experimentally would support the classical approximations used and provide an intuitive

framework for the essential physics. Further, the coherence effect might be used to differentiate between rapid and more gradual ionization models, particularly for higher- Z atoms, providing a new window into the ionization process.

ACKNOWLEDGMENTS

This work is supported by the National Science Foundation under Grant No. 2207737. We appreciate helpful discussions with Barry Walker.

-
- [1] L. D. Landau and E. M. Lifshitz, *The Classical Theory of Fields*, 1st ed. (Addison-Wesley, London, 1951), pp. 120–121.
- [2] Vachaspati, Harmonics in the scattering of light by free electrons, *Phys. Rev.* **128**, 664 (1962).
- [3] E. S. Sarachik and G. T. Schappert, Classical theory of the scattering of intense laser radiation by free electrons, *Phys. Rev. D* **1**, 2738 (1970).
- [4] A. K. Puntajer and C. Leubner, Classical versus semiclassical predictions for harmonic generation in laser-free electron scattering under experimentally realizable conditions, *J. App. Phys.* **67**, 1606 (1990).
- [5] U. Mohideen, H. W. K. Tom, R. R. Freeman, J. Bokor, and P. H. Bucksbaum, Interaction of free electrons with an intense focused laser pulse in Gaussian and conical axicon geometries, *J. Opt. Soc. Am. B* **9**, 2190 (1992).
- [6] E. Esarey, S. K. Ride, and P. Sprangle, Nonlinear Thomson scattering of intense laser pulses from beams and plasmas, *Phys. Rev. E* **48**, 3003 (1993).
- [7] C. I. Castillo-Herrera and T. W. Johnston, Incoherent harmonic emission from strong electromagnetic waves in plasmas, *IEEE Trans. Plasma Sci.* **21**, 125 (1993).
- [8] S. K. Ride, E. Esarey, and M. Baine, Thomson scattering of intense lasers from electron beams at arbitrary interaction angles, *Phys. Rev. E* **52**, 5425 (1995).
- [9] F. V. Hartemann, S. N. Fochs, G. P. Le Sage, N. C. Luhmann Jr., J. Woodworth, M. D. Perry, Y. J. Chen, and A. K. Kerman, Nonlinear ponderomotive scattering of relativistic electrons by an intense laser field at focus, *Phys. Rev. E* **51**, 4833 (1995).
- [10] Y. I. Salamin and F. H. M. Faisal, Harmonic generation by superintense light scattering from relativistic electrons, *Phys. Rev. A* **54**, 4383 (1996).
- [11] Y. I. Salamin and F. H. M. Faisal, Generation of Compton harmonics by scattering linearly polarized light of arbitrary intensity from free electrons of arbitrary initial velocity, *J. Phys. A* **31**, 1319 (1998).
- [12] Y. Li and S. V. Milton, *Intensity and pulse shape effect on the spectra and the angular distribution of nonlinear Thomson scattering*, *Summaries of Papers Presented at the Lasers and Electro-Optics, CLEO '02*, OSA, Technical Digest (IEEE, Piscataway, NJ, 2002).
- [13] Q.-H. Park, R. W. Boyd, J. E. Sipe and A. L. Gaeta, Theory of relativistic optical harmonic generation, *IEEE J. Sel. Top. Quantum Electron.* **8**, 413 (2002).
- [14] Y. Lau, F. He, D. Umstadter and R. Kowalczyk, Non-linear Thomson scattering: A tutorial, *Phys. Plasmas* **10**, 2155 (2003).
- [15] J. Gao, Thomson scattering from ultrashort and ultraintense laser pulses, *Phys. Rev. Lett.* **93**, 243001 (2004).
- [16] G. A. Krafft, Spectral distributions of Thomson-scattered photons from high-intensity pulsed lasers, *Phys. Rev. Lett.* **92**, 204802 (2004).
- [17] M. Boca and A. Oprea, Thomson scattering in the high intensity regime, *Phys. Scr.* **83**, 055404 (2011).
- [18] S. G. Rykovanov, C. G. R. Geddes, C. B. Schroeder, E. Esarey, and W. P. Leemans, Controlling the spectral shape of nonlinear Thomson scattering with proper laser chirping, *Phys. Rev. Accel. Beams* **19**, 030701 (2016).
- [19] K. Ta Phuoc, A. Rousse, M. Pittman, J. P. Rousseau, V. Malka, S. Fritzler, D. Umstadter, and D. Hulin, X-ray radiation from nonlinear Thomson scattering of an intense femtosecond laser on relativistic electrons in a Helium plasma, *Phys. Rev. Lett.* **91**, 195001 (2003).
- [20] K. Ta Phuoc, F. Burgy, J.-P. Rousseau, and A. Rousse, Nonlinear Thomson scattering from relativistic laser plasma interaction, *Eur. Phys. J. D* **33**, 301 (2005).
- [21] M. Babzien *et al.*, Observation of the second harmonic in Thomson scattering from relativistic electrons, *Phys. Rev. Lett.* **96**, 054802 (2006).
- [22] T. Kumita, Y. Kamiya, M. Babzien, I. Ben-Zvi, K. Kusche, I. V. Pavlishin, I. V. Pogorelsky, D. P. Siddons, V. Yakimenko, T. Hirose, T. Omori, J. Urakawa, K. Yokoya, D. Cline, and F. Zhou, Observation of the nonlinear effect in relativistic Thomson scattering of electron and laser beams, *Laser Phys.* **16**, 267 (2006).
- [23] G. Sarri, D. J. Corvan, W. Schumaker, J. M. Cole, A. Di Piazza, H. Ahmed, C. Harvey, C. H. Keitel, K. Krushelnick, S. P. D. Mangles, Z. Najmudin, D. Symes, A. G. R. Thomas, M. Yeung, Z. Zhao, and M. Zepf, Ultrahigh brilliance multi-MeV γ -ray beams from nonlinear relativistic Thomson scattering, *Phys. Rev. Lett.* **113**, 224801 (2014).
- [24] K. Khrennikov, J. Wenz, A. Buck, J. Xu, M. Heigoldt, L. Veisz, and S. Karsch, Tunable all-optical quasimonochromatic Thomson x-ray source in the nonlinear regime, *Phys. Rev. Lett.* **114**, 195003 (2015).
- [25] Y. Sakai *et al.*, Observation of redshifting and harmonic radiation in inverse Compton scattering, *Phys. Rev. ST Accel. Beams* **18**, 060702 (2015).
- [26] W. Yan, C. Fruhling, G. Golovin, D. Haden, J. Luo, P. Zhang, B. Zhao, J. Zhang, C. Liu, M. Chen, S. Chen, S. Banerjee, and D. Umstadter, High-order multiphoton Thomson scattering, *Nature Photon* **11**, 514 (2017).
- [27] S.-Y. Chen, A. Maksimchuk, and D. Umstadter, Experimental observation of relativistic nonlinear Thomson Scattering, *Nature (London)* **396**, 653 (1998).
- [28] S.-Y. Chen, A. Maksimchuk, E. Esarey, and D. Umstadter, Observation of phase-matched relativistic harmonic generation, *Phys. Rev. Lett.* **84**, 5528 (2000).
- [29] M. Inuma, K. Matsukado, I. Endo, M. Hashida, K. Hayashi, A. Kohara, F. Matsumoto, Y. Nakanishi, S. Sakabe, S. Shimizu, T. Tauchi, K. Yamamoto, and T. Takahashi, Observation of second harmonics in laser–electron scattering using low energy electron beam, *Phys. Lett. A* **346**, 255 (2005).
- [30] C. Z. He, A. Longman, J. A. Pérez-Hernandez, M. de Marco, C. Salgado, G. Zeraouli, G. Gatti, L. Roso, R. Fedosejevs, and W. T. Hill, III, Towards an *in situ*, full-power gauge of the

- focal-volume intensity of petawatt-class lasers, *Opt. Express* **27**, 30020 (2019).
- [31] B. Pratt, N. Atkinson, D. Hodge, M. Romero, C. Schulzke, Y. Sun, M. Ware, and J. Peatross, Experimental confirmation of electron figure-8 motion in a strong laser field, *Phys. Rev. A* **103**, L031102 (2021).
- [32] M. Romero, L. Robins, A. Stevens, N. Sa, Y. Sun, M. Ware, and J. Peatross, Nonlinear Thomson scattering: Velocity asymmetry inherent in electron figure-8 motion, *Opt. Express* **32**, 33950 (2024).
- [33] S. Augst, D. Strickland, D. D. Meyerhofer, S. L. Chin, and J. H. Eberly, Tunneling ionization of Noble gases in a high-intensity laser field, *Phys. Rev. Lett.* **63**, 2212 (1989).
- [34] E. A. Chowdhury and B. C. Walker, Multielectron ionization processes in ultrastrong laser fields, *J. Opt. Soc. Am. B* **20**, 109 (2003).
- [35] A. DiChiara, I. Ghebregziabher, S. Palaniyappan, E. L. Huskins, A. Falkowski, D. Pajeroski, and B. C. Walker, Many electron ionization processes in strong and ultrastrong fields, in *Progress in Ultrafast Intense Laser Science III*, Springer Series in Chemical Physics (Springer-Verlag, Berlin, 2008), Vol. 89.
- [36] N. Delone and V. Krainov, Tunneling and barrier-suppression ionization of atoms and ions in a laser radiation field, *Phys. Usp.* **41**, 469 (1998).
- [37] X. Tong and C. Lin, Empirical formula for static field ionization rates of atoms and molecules by lasers in the barrier-suppression regime, *J. Phys. B* **38**, 2593 (2005).
- [38] D. Bauer and P. Mulser, Exact field ionization rates in the barrier-suppression regime from numerical time-dependent Schrödinger-equation calculations, *Phys. Rev. A* **59**, 569 (1999).
- [39] A. Golovanov and I. Kostyukov, Formula for the ionisation rate of an atom or ion in a strong electromagnetic field for numerical simulation, *Quantum Electron.* **50**, 350 (2020).
- [40] A. Angioi and A. Di Piazza, Quantum limitation to the coherent emission of accelerated charges, *Phys. Rev. Lett.* **121**, 010402 (2018).
- [41] J. Peatross, C. Müller, K. Z. Hatsagortsyan, and C. H. Keitel, Photo-emission of a single-electron wave-packet in a strong laser field, *Phys. Rev. Lett.* **100**, 153601 (2008).
- [42] J. P. Corson and J. Peatross, Quantum-electrodynamic treatment of photoemission by a single-electron wave packet, *Phys. Rev. A* **84**, 053832 (2011).
- [43] J. Peatross, J. P. Corson, and G. Tarbox, Classical connection between near-field interactions and far-field radiation and the relevance to quantum photoemission, *Am. J. of Phys.* **81**, 351 (2013).
- [44] M. Ware, E. Cunningham, C. Coburn, and J. Peatross, Measured photoemission from electron wave packets in a strong laser field, *Opt. Lett.* **41**, 689 (2016).
- [45] A. Perelemov, V. Popov, and M. Terent'ev, Ionization of atoms in an alternating electric field, *Sov. Phys. JETP* **23**, 924 (1966).
- [46] M. Ammosov, N. Delone, and V. Krainov, Tunnel ionization of complex atoms and of atomic ions in an alternating electromagnetic field, *Sov. Phys. JETP* **64**, 1191 (1986).
- [47] D. Fittinghoff, Optical field ionization of atoms and ions using ultrashort laser pulse, Ph.D. thesis, Lawrence Livermore National Laboratory, 1993.
- [48] W. L. Erikson and S. Singh, Polarization properties of Maxwell-Gaussian laser beams, *Phys. Rev. E* **49**, 5778 (1994).
- [49] J. Peatross, M. Berrondo, D. Smith, and M. Ware, Vector fields in a tight laser focus: Comparison of models, *Opt. Express* **25**, 13990 (2017).
- [50] B. Quesnel and P. Mora, Theory and simulation of the interaction of ultraintense laser pulses with electrons in vacuum, *Phys. Rev. E* **58**, 3719 (1998).
- [51] M. Lewenstein, Ph. Balcou, M. Yu. Ivanov, A. L'Huillier, and P. B. Corkum, Theory of high-harmonic generation by low-frequency laser fields, *Phys. Rev. A* **49**, 2117 (1994).
- [52] L. Morgovsky, Drift mechanism of laser-induced electron acceleration in vacuum, *Laser Phys.* **25**, 126002 (2015).
- [53] J. D. Jackson, *Classical Electrodynamics*, 3rd ed. (Wiley, New York, 1998), Eq. (14.14).
- [54] G. Mainfray and C. Manus, Multiphoton ionization of atoms, *Rep. Prog. Phys.* **54**, 1333 (1991).
- [55] D. Seipt *et al.*, Analytical results for nonlinear Compton scattering in short intense laser pulses, *J. Plasma Phys.* **82**, 655820203 (2016).